Ab initio lattice dynamics and thermodynamics of rare-earth hexaborides LaB_6 and CeB_6

Tanju Gürel[1] and Resul Eryiğit[2]
[1]*Department of Physics, Namik Kemal University, Tekirdağ 59030, Turkey*
[2]*Department of Physics, Abant Izzet Baysal University, Bolu 14280, Turkey*
(Received 24 May 2010; revised manuscript received 11 August 2010; published 14 September 2010)

We have performed an *ab initio* study of structural, elastic, lattice-dynamical, and thermodynamical properties of rare-earth hexaborides LaB_6 and CeB_6. The calculations have been carried out within the density-functional theory and linear-response formalism using pseudopotentials and a plane-wave basis. Thermodynamical properties of LaB_6 and CeB_6 obtained from quasiharmonic approximation are in a good agreement with the available experimental data. We also present the complete phonon-dispersion curves, phonon density of states, and mode-Grüneisen parameters and compared with the experimental measurements. A sizable difference between the vibrational contribution to entropy of LaB_6 and CeB_6 is found. The thermal electronic contribution to entropy and specific heat is found to be important for CeB_6.

DOI: 10.1103/PhysRevB.82.104302 PACS number(s): 63.20.dk, 65.40.−b

I. INTRODUCTION

Rare-earth hexaborides (RB_6) have been attracting much attention because of their interesting electronic and magnetic properties, which include metallic, semiconducting (EuB_6, YbB_6),[1] superconducting [YB_6 (Ref. 2)], fluctuating valence [SmB_6 (Ref. 3)], and heavy fermion behavior [CeB_6 (Ref. 4)]. These wide range of properties result from a complicated interplay between the lattice structure and the lattice-dynamical and electronic properties of RB_6's. RB_6 compounds crystallize in cubic CsCl structure (space group O_h^1) with rare-earth atoms occupying the cube corners while boron octahedra at the body-center position. In such a structure, each rare-earth atom is surrounded by eight boron octahedra. This unique cage structure of the RB_6's has important implications on their lattice-dynamical properties which determine their thermodynamical behavior to a great extent. Along these lines, Mandrus *et al.*[5] have shown that the temperature dependence of the specific heat and resistivity of LaB_6 could be explained well by using a model of La ions as independent Einstein oscillators embedded in a Debye framework of boron ions.

The structural, elastic, vibrational, and thermodynamical properties of LaB_6 and CeB_6 have been investigated experimentally by several groups. But the results are sometimes contradictory or insufficient. Detailed Raman-scattering investigation of divalent and trivalent hexaborides has been reported by Refs. 6–8. The lattice dynamics of RB_6 compounds show a number of peculiar features, such as very flat acoustic mode dispersion along most of the high-symmetry directions of the Brillouin zone (BZ) and an observation of a low-frequency Raman-active mode which is not expected based on the symmetry considerations.[6] This mode has been assigned to defect or two-phonon scattering which involves zone-boundary LA modes. Various significantly different values have been reported for the measured elastic compliance constants for CeB_6, especially C_{12}, in the literature; Ref. 9 gives $C_{12}=-93$ GPa while Nakamura *et al.*[10] report a value of 53 GPa for the same constant. There are, also, similar but smaller differences among the various experimental reports on the bulk modulus values of the each compound [LaB_6 (Refs. 11–15) and CeB_6 (Refs. 9, 10, 16, and 17)]. Experimental phonon-dispersion curves measured with inelastic neutron scattering are reported by Smith *et al.*[18] and Kunii *et al.*[19] for LaB_6 and CeB_6, respectively. But these studies give the dispersions only for the acoustic modes and the lowest optic mode.

Thermodynamical properties, such as entropy, specific heat, thermal-expansion coefficient, and temperature-dependent equation of state (EOS) of LaB_6 and CeB_6 have been the subject of many studies over the years. The thermodynamical properties of LaB_6 has an extra importance for the analysis of the thermal properties of RB_6's because they are used as the nonmagnetic reference values to extract the magnetism related thermal properties of all the other RB_6's.[19] This practice assumes identical vibrational thermal properties for all RB_6's which needs to be proved or refuted by sound theoretical methods. Temperature-dependent specific heat as function of magnetic field and magnetic entropy of LaB_6 and CeB_6 were studied by Refs. 20 and 21.

On the theoretical side, Guo-Liang *et al.*[22] have investigated the elastic and thermal properties of LaB_6 in the framework of density-functional theory (DFT) with a quasiharmonic Debye model. Phonon and thermodynamical properties of alkali hexaborides have been studied by Shang *et al.*[23] The flatness of the acoustic branch of hexaborides and its dependence on the valence of the metal is investigated from first principles by Ref. 7.

Although there are a number of first-principles study of lattice-dynamics[7,24] and thermal properties of LaB_6 by using different approximations, there is no comparable study on CeB_6, to the best of our knowledge. So, a comparative *ab initio* study of elastically, vibrational, and thermodynamical properties of LaB_6 and CeB_6 would be helpful in understanding peculiarities of caged structures.

The thermodynamical properties of a solid are determined mostly by the vibrational degrees of freedom, since, generally the electronic degrees of freedom play a noticeable role only for metals at very high temperatures.[25] Investigations by several groups[26–29] show that first-principles DFT treatments within the quasiharmonic approximation (QHA) provide a reasonable description of the thermodynamical properties of many bulk materials below the melting point. Quasiharmonic

approximation lets one take into account the anharmonicity of the potential at the first order: vibrational properties can be understood in terms of the excitation of the noninteracting phonons. The temperature dependence of phonons is determined via thermal expansion of the volume of the material. Carrier *et al.*[29] have shown that even at high-temperature and high-pressure conditions QHA provides an efficient way to calculate reasonably accurate thermodynamical properties. In *ab initio* quasiharmonic calculations there are two main approaches; one is to compute the temperature-dependent phonon-free energy from phonon frequencies calculated at different lattice constants and find the equilibrium lattice properties by fitting an equation of state to total free energy.[28,30,31] Another approach is to calculate the phonon frequencies and their first and second volume derivatives at zero temperature and then calculate all thermal quantities in terms of these quantities by varying only the temperature of the thermal occupation number in the corresponding formula.[32] Earlier, the quasiharmonic approximation was used to calculate the thermodynamical properties of many monatomic crystals such as Si,[26] Ag,[28,30] Al,[31,32] Li,[31] Na,[31] W,[32] Cu,[33] C,[34] and Cs.[35] In addition to these elements, Grabowski *et al.*[36] have also calculated the linear thermal expansion and heat capacity of Pb, Au, Pd, Pt, Rh, and Ir. In recent years, quasiharmonic approximation has been applied with great success to more complex materials such as alloys [Al_3Li,[37] NiAl,[38] and PdTi (Ref. 38)], hydrides [TiH_2 (Ref. 39)], oxides [SiO_2,[40] ZrO_2,[41] PuO_2,[42] and MgO (Ref. 43)], perovskite $MgSiO_3$,[44] γ-Mg_2SiO_4,[45] hexaborides [CaB_6,[23] SrB_6,[23] BaB_6,[23] YbB_6 (Ref. 46)], GaN,[47] and ZnSe.[48]

In this paper, our aim is to help resolve the inconsistencies in experimental data of elastic constants and bulk modulus of lanthanum and cerium hexaborides, investigate the source of low-frequency "anomalous" Raman peak in RB_6 compounds and compare the lattice contribution to various thermodynamical properties of LaB_6 and CeB_6. Toward that end, we use the linear-response theory within density-functional theory framework with the local-density approximation (LDA) to the exchange-correlation energy to calculate the lattice structure, elastic constants, zone-center normal modes, phonon dispersions and the dispersion in mode-Grüneisen parameters, and thermal properties, such as the temperature dependence of volume expansion coefficient, bulk modulus, and heat capacity of two hexaborides; LaB_6 and CeB_6 by calculating the free energy of these materials for a series of lattice constants and fitting the resulting free energy to an equation of state at several temperatures. The paper is organized as follows. In Sec. II, a brief description of theory and technicalities of the computational procedure is given. In Sec. III, we present and discuss the results we have obtained and compare them with available experimental data. Finally, in Sec. IV, we give our conclusions.

II. THEORETICAL AND COMPUTATIONAL DETAILS

The EOS of a crystal at a given temperature T is constructed as[49]

$$P = -\left(\frac{\partial F}{\partial V}\right)_T, \tag{1}$$

where F is the Helmholtz free energy. In the quasiharmonic approximation, F is given by

$$F(V,T) = E(V) + F_{\mathrm{el}}(V,T) + F_{\mathrm{vib}}(\{\omega_{\mathbf{q}j}(V)\},T), \tag{2}$$

where $E(V)$ is the static contribution to the internal energy at volume V and can be easily obtained from standard DFT calculations. $F_{\mathrm{el}}(V,T)$ given in Eq. (2) is the thermal electronic contribution to free energy and is given by $F_{\mathrm{el}}=E_{\mathrm{el}}-TS_{\mathrm{el}}$. Here E_{el} is the electronic excitation energy and is given by[50]

$$E_{\mathrm{el}}(V,T) = \int n(\varepsilon,V)f(\varepsilon)\varepsilon d\varepsilon - \int^{\varepsilon_F} n(\varepsilon,V)\varepsilon d\varepsilon, \tag{3}$$

where $n(\varepsilon,V)$ is the electronic density of states (DOS) at energy ε and volume V, $f(\epsilon)$ is the Fermi distribution function. The electronic entropy S_{el} is defined as

$$S_{\mathrm{el}}(V,T) = -k_B \int n(\varepsilon,V)[f(\varepsilon)\ln f(\varepsilon) + (1-f(\varepsilon))\ln(1 - f(\varepsilon))]d\varepsilon. \tag{4}$$

Thermal electronic contribution to free energy is generally considered to be negligible away from the melting point of the material under consideration. The electronic entropy to the lowest order in temperature is estimated by Watson and Weinert as[51]

$$S_{\mathrm{el}} = \frac{\pi^2}{3} n(\varepsilon_F) k_B^2 T, \tag{5}$$

where $n(\varepsilon_F)$ is the electronic DOS at the Fermi level. So for materials with a high DOS at the Fermi energy, one would expect a sizeable contribution from the electronic degrees of freedom which is found to be the case for CeB_6 and discussed below in Sec. III.

F_{vib} in Eq. (2) is the vibrational contribution to free energy and is given by

$$F_{\mathrm{vib}}(\{\omega_{\mathbf{q}j}(V)\},T) = k_B T \int_0^{\omega_L} \ln\left(2\sinh\frac{\hbar\omega}{2k_B T}\right) g(\omega)d\omega, \tag{6}$$

where k_B is the Boltzmann constant, ω_L is the largest phonon frequency, and $g(\omega)$ is the phonon density of states

$$g(\omega) = \sum_{\mathbf{q}j} \delta[\omega - \omega_{\mathbf{q},j}(V)], \tag{7}$$

where $\omega_{\mathbf{q},j}(V)$ is the frequency of the jth phonon mode at the wave vector $\mathbf{q}$ in BZ at lattice volume V, and $\delta(\cdots)$ is the Dirac delta function. In the actual calculations, the Dirac delta function in Eq. (7) is approximated by a Gaussian of width ~ 1 meV, and the sum over the $\mathbf{q}$ is carried out over a dense k grid which will be discussed at the end of this section.

The specific-heat capacity at constant volume in the quasiharmonic approximation is the sum of a vibrational contribution,

$$C_v^{(\mathrm{vib})} = k_B \int_0^{\omega_L} \left(\frac{\hbar\omega}{2k_B T}\right)^2 \mathrm{csch}^2\left(\frac{\hbar\omega}{2k_B T}\right) g(\omega)d\omega \tag{8}$$

and an electronic contribution

$$C_v^{(\mathrm{el})} = T\left(\frac{\partial S_{\mathrm{el}}}{\partial T}\right)_V. \tag{9}$$

Due to anharmonicity, the heat capacity at a constant pressure, C_p, is different from the heat capacity at a constant volume, C_v. At high temperatures, C_v goes to a constant which is given by classical equipartition law: $C_v \approx 3Nk_B$, where N is the number of atoms in the system while C_p, which is what experiments determine directly, is proportional to T. C_p can be obtained from C_v by

$$C_p = C_v + \alpha_v^2 BVT, \tag{10}$$

where α_v is the volume thermal-expansion coefficient and B is the bulk modulus which is given by

$$B(T) = V\left(\frac{\partial^2 F}{\partial V^2}\right)_T. \tag{11}$$

The vibrational contribution to the entropy of the crystal is given by

$$S_{\mathrm{vib}} = k_B \int_0^{\omega_L} \left[\frac{\hbar\omega}{2k_BT}\coth\frac{\hbar\omega}{2k_BT} - \ln\left(2\sinh\frac{\hbar\omega}{2k_BT}\right)\right] g(\omega)d\omega. \tag{12}$$

The present results have been obtained thanks the use of the ABINIT code,[52] which is based on pseudopotentials and plane waves. It relies on an efficient fast Fourier transform algorithm[53] for the conversion of wave functions between real and reciprocal space, on the adaptation to a fixed potential of the band-by-band conjugate-gradient method,[54] and on a potential-based conjugate-gradient algorithm for the determination of the self-consistent potential.[55] Technical details of computation of responses to atomic displacements and subsequent computation of dynamical matrices can be found in Refs. 56 and 57 while the calculation of elastic constants in the linear-response framework are given in Ref. 58.

The interaction between the valence electrons and nuclei and core electrons is described by using Troullier-Martins[59] and optimized type pseudopotentials. As the exchange-correlation potential we use the LDA of Perdew-Wang[60] functional. Spin polarization is not considered in the present study. Lanthanum, cerium, and boron pseudopotentials are generated by using the OPIUM code.[61] We have treated the 5*s* (2.02), 5*p* (2.02), 5*d* (2.02), and 6*s* (2.19) electrons of La, the 5*p* (1.82), 5*d* (1.89), 4*f* (2.19), and 6*s* (2.75) electrons of Ce, and the 2*s* (1.14) and 2*p* (1.49) electrons of B as valance configurations with corresponding cutoff radii in atomic units.

For both LaB_6 and CeB_6, integrations over the Brillouin-zone volume are found to converge for a mesh of a $4\times4\times4$ Monkhorst-Pack grid[62] which corresponds to four points in the irreducible zone. In order to deal with possible convergence problems for metals, Fermi-Dirac scheme with smearing parameter σ=0.02 Ha is used. The cutoff energies of 35 and 55 Ha were found to be enough for convergence of all the reported quantities for LaB_6 and CeB_6, respectively. Phonon dynamical matrices were computed *ab initio* for a $4\times4\times4$ **q** point mesh; Fourier interpolation was then used to obtain the dynamical matrices on a $64\times64\times64$ **q** point mesh, which is used for the calculation of all quantities that involve an integration over the phonon modes. This mesh is

TABLE I. Calculated lattice parameter a_0 (in Å) and positional parameter of boron atoms x_B for LaB_6 and CeB_6 given with experimental results. Zero-temperature theoretical lattice constants are calculated without including zero-point effect.

		Experimental		Theoretical	
Material	Temperature (K)	a_0 (Å)	x_B	a_0 (Å)	x_B
LaB_6	0			4.1277	0.1997
	10	4.1527[a], 4.15112[b]	0.1993[a]	4.1429	
	50	4.15121[b]		4.1431	
	100	4.1528[a], 4.15168[b]	0.1994[a]	4.1436	
	200	4.1542[a], 4.15345[b]	0.1994[a]	4.1452	
	300	4.1561[a], 4.15553[b]	0.1995[a]	4.1474	
CeB_6	0			4.1542	0.2002
	10	4.13493[c]		4.1692	
	60	4.13522[c]		4.1694	
	100	4.13562[c], 4.1323[d]	0.19909[d]	4.1697	
	220	4.13740[c]		4.1715	
	298	4.1397[d]	0.19923[d]	4.1731	
	300	4.13899[c]		4.1731	

[a]Reference 64.
[b]Reference 65.
[c]Reference 66.
[d]Reference 67.

TABLE II. Bulk Modulus B_0 (in GPa), pressure derivative of the bulk modulus B_0', and elastic compliance constants (in GPa) of LaB_6 and CeB_6.

	Method	B_0	B_0'	C_{11}	C_{12}	C_{44}
LaB_6	This work	180	3.79	466	37	88
	Expt. (Ref. 11)	163		453.3	18.2	90.1
	Expt. (Ref. 12)	172				
	Expt. (Ref. 13)	188		478	43	84
	Expt. (Ref. 14)	142 ± 15				
	Expt. (Ref. 15)	184		463	45	89
	Expt. (Ref. 68)	164 ± 2, 173 ± 7				
	Calc. (Ref. 15)	185				
	Calc. (Ref. 22)	182.4				
CeB_6	This work	173	3.91	452	34	98
	Expt. (Ref. 16)	166	3.15			
	Expt. (Ref. 10)	191		472	53	78
	Expt. (Ref. 9)			406	–93	78
	Expt. (Ref. 17)	168		473	16	81
	Expt. (Ref. 17)	182		508	19	79

found to be satisfactory for the convergence of the calculation of thermal quantities.

To summarize, the following quantities were obtained from DFT and density-functional perturbation-theory (DFPT) calculations: (i) total energies at a range of lattice constants and (ii) for each lattice constant, the dynamical matrices for the $4\times4\times4$ set of **q** points; Fourier interpolation was used to obtain the dynamical matrices on the $64\times64\times64$ set of **q** points. This set of results was then used to calculate the thermal behavior, as described below. The thermal electronic contribution to the free energy and electronic entropy calculations are found to converge with a $16\times16\times16$ k-point sampling and Gaussian smearing of width 0.001 Ha.

III. RESULTS AND ANALYSIS

A. Atomic structure and lattice parameters

Rare-earth hexaborides crystallize in cubic CsCl-type structure which belong to the space group $O_h^1(Pm\bar{3}m)$. The rare-earth atom is located at the $1a$ (0, 0, 0) Wyckoff position while the octahedral boron molecule B_6 is placed in the $6f$ Wyckoff position with relative coordinate: (1/2, 1/2, x), where x is the positional parameter. The primitive unit cell contains seven atoms.

The static results for lattice constant a_0, the bulk modulus B_0, and the pressure derivative of the bulk modulus B_0' are obtained by fitting the static total energies versus lattice constant to Vinet equation of state,[63]

$$E(V) = E_0 + 9B_0V_0(e^{A(1-x)}[A^{-1}(1-x) - A^{-2}] + A^{-2}), \tag{13}$$

where V_0 is the equilibrium volume, $x=(V/V_0)^{1/3}$, B_0 is the bulk modulus, and $A=3(B_0'-1)/2$, where B_0' is the pressure derivative of the bulk modulus. The temperature-dependent parameters of EOS (E_0, V_0, B_0, and B_0') are obtained from least-squares fitting procedure. They can be used to calculate the temperature-dependent pressure-volume relations and pressure and temperature dependence of bulk modulus as[63]

$$P(V) = \left[\frac{3(1-x)}{x^2}\right]B_0e^{A(1-x)} \tag{14}$$

and

$$B(P) = -B_0e^{[A(1-x)]}[(1-A)x^{-1} - 2x^{-2} + A]. \tag{15}$$

Table I shows the equilibrium lattice parameter a_0 and positional parameter x for the materials LaB_6 and CeB_6 along with some experimental data in different temperatures. Considering the exclusion of the zero-point effects at zero temperature the calculated quantities of the present work are in a very good agreement with the experimental ones. The calculated lattice parameter of LaB_6 has 0.6% and of CeB_6 has only 0.5% discrepancy with the measurements.

The calculated and experimental bulk moduli, its pressure derivative and elastic constants are given in Table II. Experimental results given in the table show large discrepancies among themselves partly because of different techniques used in obtaining them. For LaB_6, the calculated bulk modulus of the present study best agrees with the recent study of Ref. 15 with a discrepancy of about 2%. The calculated bulk modulus value of CeB_6 slightly overestimates the reported ultrasonic measurement of Lüthi *et al.*[17] For CeB_6, the experimental elastic constants study of Ref. 9 reports a negative C_{12} value which was not found in our calculations or in other experiments.[10,17] Our calculated elastic constants of LaB_6 and CeB_6 are comparable with each other.

TABLE III. The Brillouin-zone-center phonon frequencies (in cm^{-1}) and mode-Grüneisen parameters (γ) of LaB_6 and CeB_6.

		$A_{1g}(R)$	$E_g(R)$	$T_{2g}(R)$	$T_{1u}(IR)$	$T_{1u}(IR)$	T_{1g}	T_{2u}
LaB_6	This work	1273	1116	694	848	176	576	503
	Expt. (Ref. 69)	1258	1120	682				
	Expt. (Ref. 70)	1245	1115	675				
	Expt. (Ref. 71)	1240	1152-1112	690-670	1095-1070	210-170	533-500-460	790-700
	Expt. (Ref. 14)	1251	1116	677		186	438	
	Expt. (Ref. 68)	1253	1129	678				
γ	This work	1.41	1.32	1.07	1.09	2.76	0.12	1.25
	Expt. (Ref. 14)	1.1	1.0	0.8		−0.6	2.1	
	Expt. (Ref. 68)	1.53	1.21	0.99				
CeB_6	This work	1228	1083	695	835	193	582	497
	Expt. (Ref. 72)	1270	1142	680				
	Expt. (Ref. 73)				866			
γ	This work	1.45	1.36	0.95	1.04	2.38	0.08	1.26

B. Phonons

1. Normal modes at the Brillouin-zone center

In rare-earth hexaborides, the primitive cell contains seven atoms, giving rise to 21 normal modes. The group theory analysis allows decomposing the vibrations at the Γ point as

$$\Gamma = A_{1g} \oplus E_g \oplus T_{1g} \oplus T_{2g} \oplus 3T_{1u} \oplus T_{2u}.$$

One of the T_{1u} modes is acoustic mode and corresponds to a pure translation of the whole crystal. Three of the optical modes with symmetries A_{1g}, E_g, and T_{2g} are Raman (R) active. The remaining two T_{1u} modes are infrared (IR) active, T_{1g} and T_{2u} modes are optically inactive.

In Table III we have presented the calculated Brillouin-zone-center phonon frequencies and mode-Grüneisen parameters along with the available experimental data. As it is clear from the table, for both of the materials, our results are in good agreement with the experimental ones except in some modes with those reported by Ref. 71. For the frequencies that have an experimental counterpart, the error is equal or less than 5%. This difference is much smaller for LaB_6 ($\leq$1.7%). In the Raman-scattering measurements, it was found that the frequencies of the A_{1g} and E_g modes of hexaborides decrease systematically with increasing lattice constant.[69,72] Experimentally, Raman frequencies (lattice constant) of the CeB_6 is somewhat higher (lower) than LaB_6. In our calculations, to obtain phonon frequencies of these materials, we have used the theoretical lattice constants which was found to be higher for LaB_6. Because of that, in our results the frequencies of the aforementioned Raman modes of CeB_6 are found to be lower than those of LaB_6 contrary to the experiments. The experimental mode-Grüneisen parameters of the Raman study of Teredesai *et al.*[14] is about 30% lower than our calculated ones but considering the recent high-pressure Raman study of Godwal *et al.*[68] the discrepancy is only around 8%.

The displacement patterns of the Brillouin-zone-center modes are given in Fig. 1 together with the symbols for the irreducible representations. The degenerate modes are represented only once. One of the T_{1u} mode corresponds to the acoustic phonon with displacement of the whole lattice to the same direction. The other T_{1u} is the only optical mode that the boron octahedra move undeformed. The rest of the modes are associated with deformations of the boron octahedra. The breathing A_{1g} mode and E_g modes are B-B bond-stretching modes. The deformations of these modes are particularly large so they have the highest frequencies.

2. Static-dispersion curves, phonon density of states, and mode-Grüneisen parameters

In this section we present the results of phonon-dispersion curves, phonon density of states, and dispersion in mode-Grüneisen parameters calculated at the theoretical equilibrium volume. The calculated phonon-dispersion curves and phonon density of states for LaB_6 and CeB_6 are displayed in Figs. 2 and 3, respectively, along with the available experimental[18,19] and theoretical[24] results. The dispersion curves are showed along the high-symmetry direction X-Γ-R-M-Γ of the Brillouin zone.

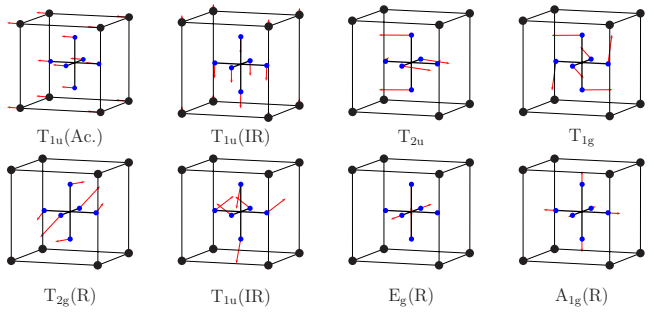

FIG. 1. (Color online) Eigendisplacement patterns of the normal modes of hexaborides at the Brillouin-zone center. (R: Raman active, IR: infrared active, and Ac.: acoustic modes.)

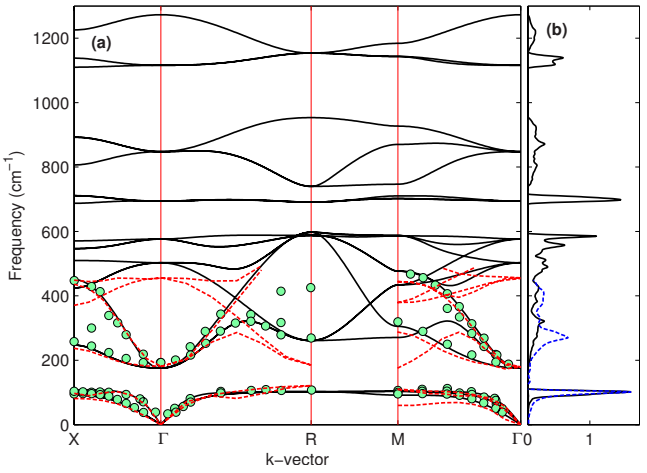

FIG. 2. (Color online) (a) Phonon-dispersion relations of LaB_6. Solid lines show the results of the present study and the dashed lines are the frozen-phonon calculations of Monnier and Delley (Ref. 24). Experimental values (circles) are taken from Smith *et al.* (Ref. 18). (b) Phonon density of states of LaB_6. Solid lines show the results of the present study and the dashed lines are obtained by Kunii (Ref. 74) using the experimental-dispersion relation of Smith *et al.* (Ref. 18).

The details of the calculation of phonon density of states and thermodynamical quantities are explained in Ref. 40. Phonon density of states is obtained by a root sampling (or histogram) method. Sampling a $64\times64\times64$ Monkhorst-Pack grid for phonon wave vectors **q** is found to be sufficient in order to get the mean relative error in each channel of phonon density of states.

For both LaB_6 and CeB_6, experimental phonon-dispersion frequencies are available only up to 480 cm^{-1} and have a good agreement with the calculated results as can be seen from Figs. 2 and 3. The rapid flattening of the dispersion of the acoustic modes away from the center of the BZ is described excellently which was not achieved by the previous *ab initio* investigation of the phonons of LaB_6 by Monnier and Delley.[24] The differences showed in Fig. 2 are probably due to the basis set limitation or *k*-point setting in the calculations of Monnier and Delley.[24] For both Figs. 2 and 3, the discrepancies between the calculated and measured phonon frequencies at the R point around ~400 cm^{-1} might occur from two possibilities: as it is also conjectured by Ref. 24, neutron measurements around the BZ boundaries might have had problems because of the sample size and lower neutron flux available at higher energies. Another possibility is that there might be some processes that cannot be accounted in the framework of DFPT around R point.

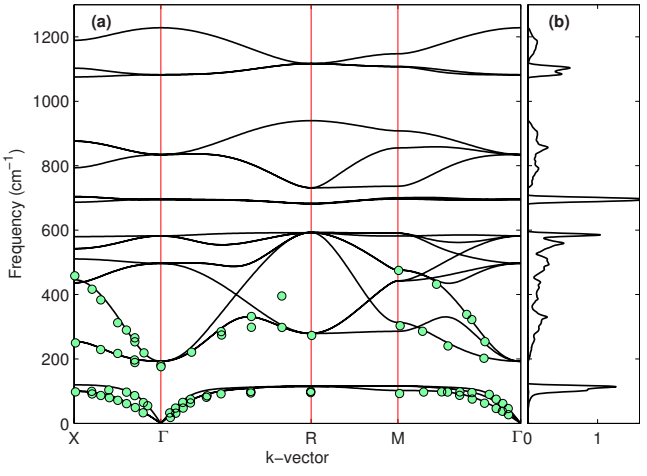

FIG. 3. (Color online) (a) Phonon-dispersion relations of CeB_6. Solid lines show the results of the present study and experimental values (circles) are taken from Kunii *et al.* (Ref. 19). (b) Phonon density of states of CeB_6 calculated in this study.

The available experimental and theoretical data are very limited for phonon density of states. Kunii[74] obtained the density of states of LaB_6 by point-contact spectroscopy where the peaks are situated around 97, 194, 306, and 403 cm^{-1}. In that study, phonon density of states is also calculated from the neutron-scattering experiment done by Smith *et al.*[18] Schell *et al.*[75] have also obtained similar peaks from inelastic-neutron-scattering experiment on polycrystalline LaB_6. Our calculated results are compatible with the reported peaks in Refs. 74 and 75 except 194 cm^{-1} peak which was also not observed in neutron-scattering experiment of Smith *et al.*[18]

The anharmonicity of the vibrations can be examined by computing the mode-Grüneisen parameters, defined for the mode λ at the wave vector **q** by

$$\gamma_{\mathbf{q}\lambda} = -\frac{V}{\omega_{\mathbf{q}\lambda}(V)}\frac{\partial\omega_{\mathbf{q}\lambda}(V)}{\partial V}, \tag{16}$$

where V is the volume of the unit cell. Negative mode-Grüneisen parameters correspond to a decrease in the mode frequency with decreasing volume and are indicative of structural phase transitions. Also negative $\gamma_{\mathbf{q}\lambda}$ might lead to negative thermal expansion. The mode-Grüneisen parameters of LaB_6 and CeB_6 are found to be positive throughout the high-symmetry directions of the Brillouin zone and are displayed in Figs. 4(a) and 4(b), respectively. Since the acoustic branches vanish linearly with a slope depending on the direction of approach to the Brillouin-zone center, the corresponding mode-Grüneisen parameters are discontinuous at the Γ point. The $\gamma_{\mathbf{q}\lambda}$'s for the optical branches are found to be very similar in shape and magnitude for LaB_6 and CeB_6 while the acoustic mode-Grüneisen parameters of LaB_6 are consistently higher than those of CeB_6 along the whole region of the Brillouin zone as shown in Fig. 4. One prominent feature of the Raman spectroscopy of RB_6's is a low-frequency mode which has strong intensity at room temperature but disappears at very low temperatures. This mode, which should not be Raman active based on symmetry considerations, was originally observed at around 200 cm^{-1} and assigned to optical T_{1u} mode[76] while later it was attributed to the two-phonon scattering by the BZ boundary LA phonons by Ogita *et al.*,[6] among others. Based on a comparison of the frequency of this mode versus the lattice constant for different RB_6's, it was conjectured that the mode is anomalous, i.e., its frequency decreases with decreasing lattice constant. The calculated zone-boundary LA phonon frequencies for LaB_6 (CeB_6) are 108, 103, and 104 (110, 115, and 116) cm^{-1} at X, R, and M points, respectively. They are, consistently,

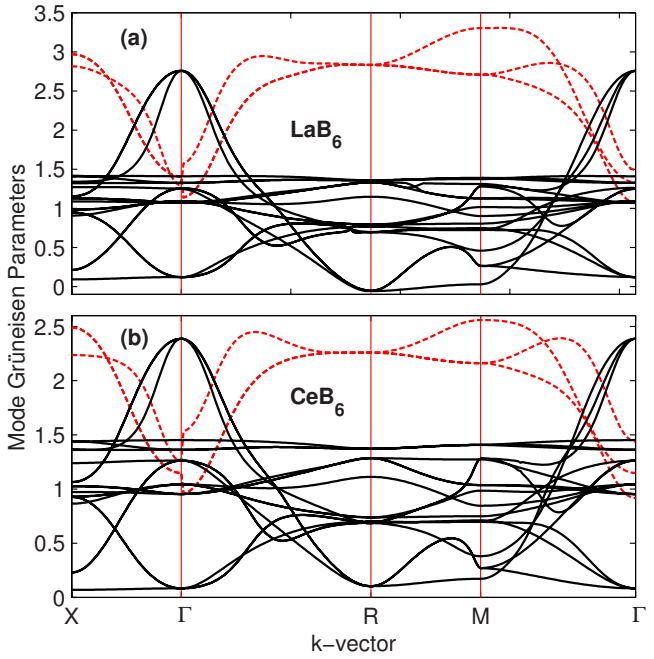

FIG. 4. (Color online) The calculated mode-Grüneisen parameters of (a) LaB_6 and (b) CeB_6. Dashed lines are the acoustic modes and solid lines are the optical modes.

higher for CeB_6 than for LaB_6 which is inline with the experimental case. But, our calculated positive acoustic mode-Grüneisen parameters for both LaB_6 and CeB_6 indicate that there is no anomaly in volume dependence of the zone-boundary acoustic modes. This finding does not rule out the two-photon scattering possibility for the observed mode but it calls into question the argument used by Ref. 6 to account for the decreasing mode frequency with decreasing cage space of the rare-earth atom. Findings of the present study indicate that the observed behavior depends on the difference in interaction between the rare-earth ion and the boron framework rather than the different cage space in each RB_6.

C. Thermodynamical properties

Temperature-dependent phonon contributions to Helmholtz free energy $\Delta F_{\text{vib}}[\omega_{\mathbf{q}j}(V),T]$ of LaB_6 and CeB_6, computed from Eq. (6), are displayed in Figs. 5(a) and 5(b), respectively. These calculations are done at the relevant static equilibrium lattice constant. Because of zero-point motion, the zero-temperature value of ΔF does not vanish. This quantity can be calculated from the asymptotic expression of Eq. (6) as

$$\Delta F_0 = \int_0^{\omega_L} \frac{\hbar\omega}{2} g(\omega) d\omega. \tag{17}$$

Calculated effect of zero-point energy upon the volume and bulk modulus for LaB_6 is $\Delta V_0/V_0=0.011$ and $\Delta B_0/B_0=-0.026$. Similarly for CeB_6 we find, $\Delta V_0/V_0=0.011$ and $\Delta B_0/B_0=-0.025$. The zero-point energy corrected equilibrium lattice constant of LaB_6 (CeB_6) is 4.145 Å (4.171 Å) which is closer (further) to the experimental low-temperature value of 4.153 Å (Ref. 64) [4.132 Å (Ref. 67)] than the noncorrected value. The correction to the bulk modulus is within the range of differences between the different experimental reports.

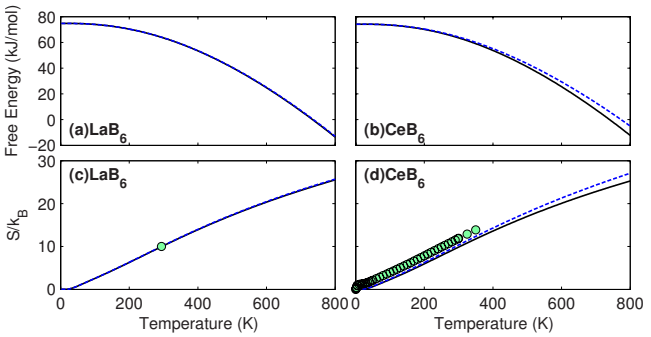

FIG. 5. (Color online) Vibrational contribution to Helmholtz free energy for (a) LaB_6 and (b) CeB_6 and vibrational contribution to entropy for (c) LaB_6 and (d) CeB_6 together with experimental results (circles) of Refs. 77 and 80 for LaB_6 and CeB_6, respectively. The solid (dotted) lines show the vibrational (vibrational plus thermal electronic) contributions.

The vibrational and the sum of vibrational and electronic entropy of LaB_6 and CeB_6 are calculated from Eqs. (4) and (12) and displayed in Figs. 5(c) and 5(d), respectively. It is clear from Fig. 5(c) that the electronic contribution to the entropy for LaB_6 is small and the sum and the vibrational contributions are indistinguishable in the plot (S_{el} reaches $1.5k_B$ at 800 K for LaB_6). On the other hand, S_{el} for CeB_6 is sizeable as can be discerned from Fig. 5(d). The room-temperature experimental entropy data ($S_{RT}=10k_B$) for LaB_6 exists[77,78] and is in perfect agreement with our calculated value ($S_{RT}=10.11k_B$), as can be seen from Fig. 5(c). S_{RT} of CeB_6 is measured as $11.8k_B$ by Muratov *et al.*[79] and Westrum *et al.*[80] which is about 14% higher than our computed value ($S_{RT}=10.26k_B$). The discrepancy between the experimental and the calculated values stems from the fact that our calculated value corresponds to the sum of vibrational and electronic entropy while CeB_6 has also magnetic entropy which is not accounted for in our calculations. The difference of $\sim 1.54k_B$ is close to k_B ln 6 which is the maximum magnetic entropy possible for $^2F_{5/2}$ multiplet of $4f$ electron of cerium atoms.[21,81] The magnetic contribution can also be calculated with DFT derived parameters by using a model Hamiltonian such as Heisenberg model,[82] which is not considered in the present work.

Magnetic entropy of rare-earth hexaborides with magnetic rare-earth element is obtained by subtracting the entropy of LaB_6 from that of the rare earth by assuming that the vibrational and electronic entropy of all RB_6 compounds are approximately equal.[21,81] We display the difference between the vibrational and total (vibrational+electronic) entropies of CeB_6 and LaB_6 in Fig. 6. One should note that vibrational entropy of LaB_6 is relatively higher than that of CeB_6 but the higher electronic entropy of CeB_6 makes the difference in the total entropy small. The upper portion of Fig. 6 shows temperature dependence of the magnetic entropy CeB_6 which are obtained by taking the difference between our calculated entropy and measured total entropy of CeB_6.[80] Two different

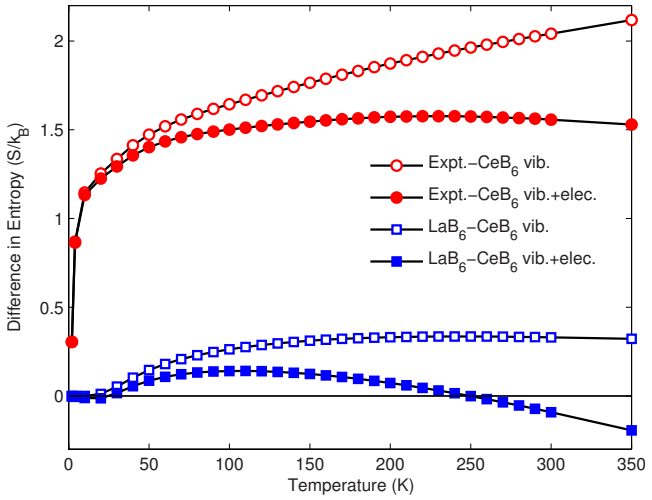

FIG. 6. (Color online) Difference between the calculated entropies of LaB_6 and CeB_6 (squares) and the difference between the experimental entropy (Ref. 80) and the calculated entropy for CeB_6 (circles).

curves correspond to the calculations including only the vibrational effects and sum of vibrational and electronic contributions. As can be seen from the figure, inclusion of the electronic entropy is crucial to obtain a constant magnetic entropy at higher temperatures.

To calculate the thermal properties, the free energy of LaB_6 and CeB_6 were calculated as a function of volume and temperature. Calculations were performed on a primitive cubic cell at a series of 11 equidistant lattice constants (4.058–4.195 Å) for LaB_6 and (4.084–4.222 Å) for CeB_6. At each different temperature we calculated the *ab initio* free energy as a function of volume, and then performed a least-squares fit of the results to a Vinet equation of state[63] [Eq. (13)]. The equilibrium volume at temperature T, $V_0(T)$ is obtained by minimizing free energy with respect to V. The volume thermal expansion is defined as

$$\eta(T) = \frac{V_0(T) - V_0(T_c)}{V_0(T_c)}, \tag{18}$$

where T_c is the reference temperature of 294 K. Our results for volume thermal expansion of LaB_6 and CeB_6 are displayed in Figs. 7(a) and 7(b), respectively. In the figure, the dotted lines represent the volume expansion calculated by considering only the vibrational degrees of freedom while the solid line represent η due to both vibrational and electronic effects while the circles are experimental data from Refs. 65 and 66. As expected, based on the free energies in Fig. 5, the electronic contribution to η for LaB_6 (CeB_6) is negligible (sizable). The overall agreement for volume thermal expansion is perfect for both materials.

The linear thermal-expansion coefficient is defined as $\alpha(T) = \frac{1}{a(T)} \frac{da}{dT}$, where $a(T)$ is the equilibrium lattice constant at temperature T. The temperature dependencies of the linear thermal-expansion coefficients for lanthanum and cerium hexaborides are given in Figs. 8(a) and 8(b), respectively. The agreement with respect to the experimental results of

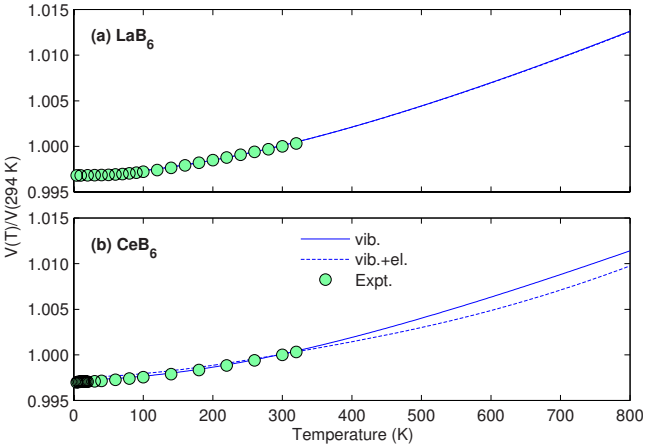

FIG. 7. (Color online) Thermal volume expansion of (a) LaB_6 and (b) CeB_6. Experimental data are taken from the studies of Sirota *et al.* with Ref. 65 for LaB_6 and Ref. 66 for CeB_6. The solid (dotted) lines represent the vibrational (vibrational plus thermal electronic) contributions.

Ref. 66 is better for LaB_6 (CeB_6) at low (high) temperatures. Including the effect of thermal electronic contributions make the agreement for CeB_6 somewhat better. There are two prominent features in the experimental low-temperature linear-expansion coefficient of CeB_6 below 10 K and around 40 K. The peak below 10 K is attributed to the Kondo effect while the peak around 40 K is thought to be related to Jahn-Teller effect or the flatness of the acoustic modes.[66] While Kondo effect is outside the scope of the present study, the calculated vibrational contribution to the expansion coefficient indicates that the peak at 40 K is not due to the lattice effects.

The temperature dependence of the bulk modulus of LaB_6 and CeB_6 are displayed in Fig. 9(a). As an expected result, bulk modulus value decreases with increasing temperature

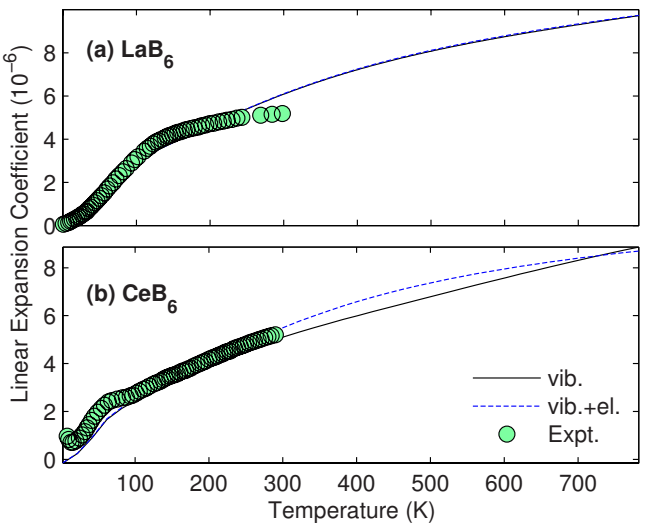

FIG. 8. (Color online) Temperature dependence of linear-expansion coefficient of LaB_6 and CeB_6. The experimental values are from the study of Sirota *et al.* (Ref. 66). The solid (dotted) lines represent the vibrational (vibrational plus thermal electronic) contributions.

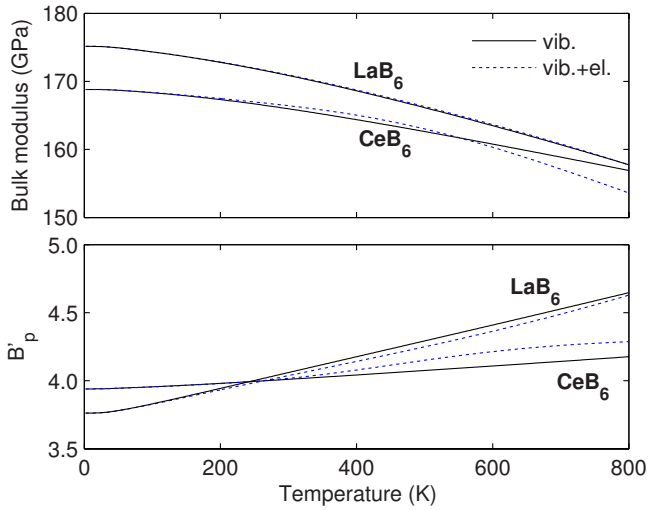

FIG. 9. (Color online) Temperature dependence of (a) bulk modulus and (b) its pressure derivative of LaB_6 and CeB_6. The solid (dotted) lines represent the vibrational (vibrational plus thermal electronic) contributions.

for both materials. Including the thermal electronic contributions increases the rate of change in B with T at higher temperatures. We have also calculated the temperature dependence of the pressure derivative of the bulk modulus and presented it in Fig. 9(b) for LaB_6 and CeB_6. Unlike bulk modulus, its pressure derivative increases with temperature and this increment is mostly linear.

In Figs. 10(a) and 10(b) we display the specific heat of LaB_6 and CeB_6, respectively. The solid (dotted) line is our result for the specific heat at constant volume (pressure). Both of Figs. 10(a) and 10(b) contain four curves denoted as C_v (vib) which is calculated from Eq. (8) and contains only the vibrational contributions, C_v (vib+el) calculated as the sum of Eqs. (8) and (9) and contains both electronic and the

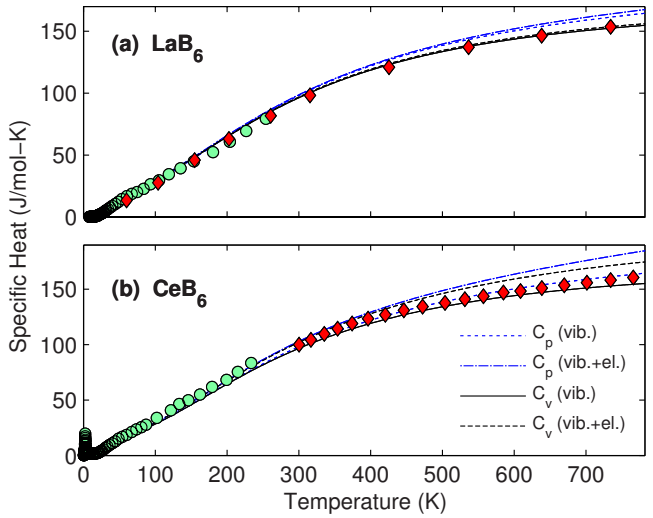

FIG. 10. (Color online) Temperature dependence of constant volume and constant pressure specific heat of (a) LaB_6 and (b) CeB_6. For LaB_6, the experimental values are from Ref. 20 (circles) and Ref. 83 (diamonds), for CeB_6 values are from Ref. 20 (circles) and Ref. 79 (diamonds).

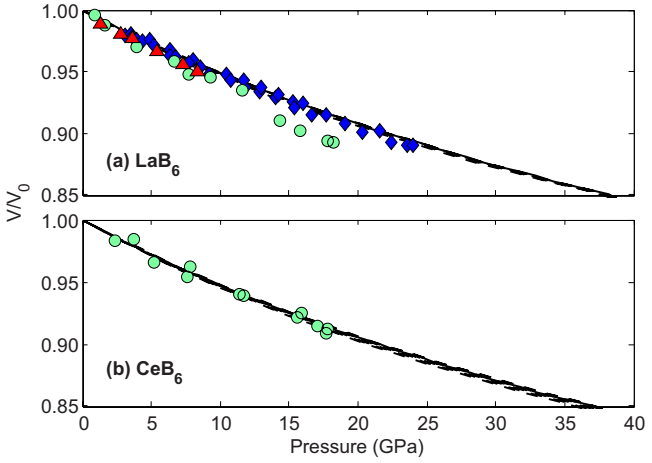

FIG. 11. (Color online) Pressure dependence of unit-cell volume of (a) LaB_6 and (b) CeB_6 at several temperatures. The solid lines in figures are for $T=294$ K. Dashed lines are separated by 100 from 0 to 800 K. The experimental values in (a) are from Ref. 12 (triangles), Ref. 14 (circles), and Ref. 68 (diamonds). The experimental values in (b) are from the study of Leger *et al.* (Ref. 16) (circles).

vibrational effects, C_p (vib) and C_p (vib+el) are the constant pressure specific heat calculated from Eq. (10) by using the corresponding C_v. To be guide to eye, we should mention that the order of these quantities from lower to higher in Fig. 10(b) is $C_v(\text{vib}) < C_p(\text{vib}) < C_v(\text{vib+el}) < C_p(\text{vib+el})$. At low temperatures, our first-principles results agree well with experiment for LaB_6 with a slight underestimation while for CeB_6 the agreement is satisfactory with a slight overestimation. At higher temperatures, for both materials, the calculated constant pressure specific heat overestimates the experimental results which is a well-known issue in *ab initio* calculations. Inclusion of thermal electronic effects makes the agreement somewhat worse at the high temperatures. In CeB_6, there exists two peaks in experimental specific-heat values at temperature lower than 20 K because of the Kondo effect which is not accessible with the methodology used in the present study.

Pressure dependence of unit-cell volume of LaB_6 and CeB_6 are displayed and compared to experimental data in Figs. 11(a) and 11(b), respectively. The solid lines in both figures are for $T=294$ K while dashed lines are for various temperatures from 2 to 800 K separated by 100 K. For both materials, pressure dependence of the unit-cell volume does not change too much with respect to temperature in the given range. In the experimental study of Teredesai *et al.*[14] it has been reported that for LaB_6, there exists a phase transition from cubic phase to orthorhombic phase at around 10 GPa, which is not observed in the recent study of Godwal *et al.*[68] For the cubic phase of two materials, the agreement between the calculated and experimental values is very good with a slight underestimation. For CeB_6, if one takes into account the spread in the experimental values of Ref. 16, the agreement is better. For LaB_6, the agreement between the experimental data of Ref. 68 and our calculated results is excellent as can be seen from Fig. 11(a).

From the results presented so far, one question concerning the *ab initio* calculation of thermodynamical quantities is the

relation between the error in calculating the static equilibrium lattice properties, such as lattice constant and bulk modulus, and ensuing error in the calculated thermodynamical quantities. While investigating the thermal properties of Cu, Narasimhan and de Gironcoli[33] suggested that a better value for the static value of a_0 and B_0 would be a good indicator of a better description of finite-temperature properties. Since the lattice constant and bulk modulus values for the materials considered in this paper are in a good agreement with experimental measurements, our calculated thermodynamical quantities give compatible results with the experimental values.

IV. CONCLUSION

We have done a comprehensive *ab initio* investigation of elastic, lattice-dynamical, and thermodynamical properties of hexaborides of La and Ce within the density-functional and density-functional perturbation-theory frameworks by using quasiharmonic approximation to account for the anharmonicity of the vibrations. LDA is found to underestimate (overestimate) the lattice constant of LaB_6 (CeB_6) by 0.5%. The calculated bulk modulus of LaB_6 is found to be slightly higher than that of CeB_6 which are both in the limits of experimentally reported values. The effect of the zero-point motion on the volume and bulk modulus of the both compounds are found to be similar; the volume is enlarged by 1.1% while the bulk modulus decreases by $\approx$2.5% compared to the no zero-point case. This finding is expected because zero-point motion can be considered as a negative pressure which causes expansion of the volume and an accompanied softening which is indicated by the decreasing bulk modulus.

Concerning the elastic constants of LaB_6 and CeB_6, we have found that the calculated C_{11} and C_{12} (C_{44}) of CeB_6 are lower (higher) than those of LaB_6. The results reported here would be helpful in resolving the great disparity in reported experimental values of C_{12}, especially for CeB_6 which is reported to be in the range −93 (Ref. 9) to 53 GPa.[10] Our calculated value is closer to that of Ref. 10.

We have computed the zone-center vibrational frequencies and their eigendisplacements and compared the results to the Raman scattering and IR measurements reported in the literature. The Raman-active modes involve displacement of boron atoms and are expected to be similar in both of the compounds because the rare-earth atoms are thought to interact weakly with the covalently bonded boron octahedra. Our results indicate that there is a appreciable effect of rare-earth boron interaction manifested in especially for the A_{1g} mode frequency of LaB_6 which is around 4% higher than that of CeB_6.

The dispersion of mode frequencies and their volume dependence along with the projected phonons density of states at zero pressure were calculated and compared to the literature data. The rapid flattening of the acoustic modes as one goes away from the center of the BZ, which is thought to have a signature in low-temperature thermal properties, is found to be well reproduced for both of the compounds. The phonon partial density of states indicate that the low-frequency sharp peak is due to motion of the rare-earth species while the higher frequency modes are almost solely due to motion of boron octahedra in various patterns. The mode-Grüneisen parameters were found to be positive across all the investigated directions which indicate that mode frequencies increase under pressure. Implication of this finding concerning the low-frequency anomalous Raman mode of RB_6 compounds is that the cage space frequency of zone-boundary acoustic mode frequency needs to be reconsidered.

The entropy and specific heat of LaB_6 is used as nonmagnetic reference data for the rare-earth hexaborides. We have investigated the vibrational and electronic entropy of LaB_6 and CeB_6 and found that the vibrational entropy of LaB_6 is appreciably higher than that of CeB_6 while for the electronic entropy the opposite is valid. As a result the difference in total entropy of the two hexaborides can be considered as a measure of the magnetic entropy of CeB_6. For the other magnetic lanthanides a similar conclusion can be reached only after an investigation of the electronic entropy.

We have also considered the temperature-dependent thermal properties such as volume thermal expansion, linear-expansion coefficient, bulk modulus and its pressure derivative, and constant volume and constant pressure specific heat. Calculated quantities were found to be in reasonable agreement with the experimental data except for the specific heat and linear-expansion coefficient of CeB_6 at low temperatures. The discrepancy is due to the Kondo effect which is not considered in the present study.

[1] J. M. Tarascon, J. Etourneau, P. Dordor, P. Hagenmuller, M. Kasaya, and J. M. D. Coey, J. Appl. Phys. **51**, 574 (1980).
[2] S. Kunii, T. Kasuya, K. Kadowaki, M. Date, and S. B. Woods, Solid State Commun. **52**, 659 (1984).
[3] P. A. Alekseev, J. M. Mignot, J. Rossat-Mignod, V. N. Lazukov, I. P. Sadikov, E. S. Konovalova, and Y. B. Paderno, J. Phys.: Condens. Matter **7**, 289 (1995).
[4] T. Komatsubara, N. Sato, S. Kunii, I. Oguro, Y. Furukawa, Y. Onuki, and T. Kasuya, J. Magn. Magn. Mater. **31-34**, 368 (1983).
[5] D. Mandrus, B. C. Sales, and R. Jin, Phys. Rev. B **64**, 012302 (2001).
[6] N. Ogita, S. Nagai, N. Okamoto, M. Udagawa, F. Iga, M. Sera, J. Akimitsu, and S. Kunii, Phys. Rev. B **68**, 224305 (2003).
[7] T. Hasegawa, N. Ogita, and M. Udagawa, J. Phys.: Conf. Ser. **176**, 012031 (2009).
[8] N. Ogita, T. Hasegawa, M. Udagawa, F. Iga, and S. Kunii, J. Phys.: Conf. Ser. **176**, 012032 (2009).
[9] T. Goto, A. Tamaki, S. Kunii, T. Nakajima, T. Fujimura, T. Kasuya, T. Komatsubarra, and S. B. Woods, J. Magn. Magn. Mater. **31-34**, 419 (1983).
[10] S. Nakamura, T. Goto, S. Kunii, K. Iwashita, and A. Tamaki, J. Phys. Soc. Jpn. **63**, 623 (1994).
[11] T. Tanaka, J. Yoshimoto, M. Ishli, E. Bannai, and S. Kawai, Solid

State Commun. **22**, 203 (1977).
[12] T. Lundström, B. Lönnberg, B. Törmä, J. Etourneau, and J. M. Tarascon, Phys. Scr. **26**, 414 (1982).
[13] S. Nakamura, T. Goto, M. Kasaya, and S. Kunii, J. Phys. Soc. Jpn. **60**, 4311 (1991).
[14] P. Teredesai, D. V. S. Muthu, N. Chandrabhas, S. Meenakshi, V. Vijayakumar, P. Modak, R. S. Rao, B. K. Godwal, S. K. Sikka, and A. K. Sood, Solid State Commun. **129**, 791 (2004).
[15] A. Baranovskiy, G. Grechnev, V. Fil, T. Ignatova, A. Logosha, A. Panfilov, I. Svechkarev, N. Shitsevalova, V. Filippov, and O. Eriksson, J. Alloys Compd. **442**, 228 (2007).
[16] J. Leger, J. Rossat-Mignod, S. Kunii, and T. Kasuya, Solid State Commun. **54**, 995 (1985).
[17] B. Lüthi, S. Blumenröder, B. Hillebrands, E. Zirngiebl, G. Güntherodt, and K. Winzer, Z. Phys. B: Condens. Matter **58**, 31 (1984).
[18] H. G. Smith, G. Dolling, S. Kunii, M. Kasaya, B. Liu, K. Takegahara, T. Kasuya, and T. Goto, Solid State Commun. **53**, 15 (1985).
[19] S. Kunii, J. Effantin, and J. Rossat-Mingnod, J. Phys. Soc. Jpn. **66**, 1029 (1997).
[20] Y. Peysson, C. Ayache, B. Salce, J. Rossat-Mignod, S. Kunii, and T. Kasuya, J. Magn. Magn. Mater. **47-48**, 63 (1985).
[21] Y. Peysson, C. Ayache, J. Rossat-Mignod, S. Kunii, and T. Kasuya, J. Phys. (Paris) **47**, 113 (1986).
[22] X. Guo-Liang, C. Jing-Dong, X. Yao-Zheng, L. Xue-Feng, L. Yu-Fang, and Z. Xian-Zhou, Chin. Phys. Lett. **26**, 056201 (2009).
[23] S. Shang, Y. Wang, and Z.-K. Liu, Phys. Rev. B **75**, 024302 (2007).
[24] R. Monnier and B. Delley, Phys. Rev. B **70**, 193403 (2004).
[25] N. W. Ashcroft and N. D. Mermin, *Solid State Physics* (Saunders College, Philadelphia, 1976).
[26] S. Biernacki and M. Scheffler, Phys. Rev. Lett. **63**, 290 (1989).
[27] P. Pavone, K. Karch, O. Schütt, W. Windl, D. Strauch, P. Giannozzi, and S. Baroni, Phys. Rev. B **48**, 3156 (1993).
[28] J. Xie, S. P. Chen, S. de Gironcoli, and S. Baroni, Philos. Mag. B **79**, 911 (1999).
[29] P. Carrier, R. Wentzcovitch, and J. Tsuchiya, Phys. Rev. B **76**, 064116 (2007).
[30] J. Xie, S. de Gironcoli, S. Baroni, and M. Scheffler, Phys. Rev. B **59**, 965 (1999).
[31] A. A. Quong and A. Y. Liu, Phys. Rev. B **56**, 7767 (1997).
[32] A. Debernardi, M. Alouani, and H. Dreyssé, Phys. Rev. B **63**, 064305 (2001).
[33] S. Narasimhan and S. de Gironcoli, Phys. Rev. B **65**, 064302 (2002).
[34] J. Xie, S. P. Chen, J. S. Tse, S. deGironcoli, and S. Baroni, Phys. Rev. B **60**, 9444 (1999).
[35] N. E. Christensen, D. J. Boers, J. L. van Velsen, and D. L. Novikov, Phys. Rev. B **61**, R3764 (2000).
[36] B. Grabowski, T. Hickel, and J. Neugebauer, Phys. Rev. B **76**, 024309 (2007).
[37] Z. Li and J. S. Tse, Phys. Rev. B **61**, 14531 (2000).
[38] G. J. Ackland, X. Huang, and K. M. Rabe, Phys. Rev. B **68**, 214104 (2003).
[39] C. Hu, D. Chen, Y. Wang, and K. Yang, J. Alloys Compd. **450**, 369 (2008).
[40] C. Lee and X. Gonze, Phys. Rev. B **51**, 8610 (1995).
[41] A. Kuwabara, T. Tohei, T. Yamamoto, and I. Tanaka, Phys. Rev. B **71**, 064301 (2005).
[42] S. Minamoto, M. Kato, K. Konashi, and Y. Kawazoe, J. Nucl. Mater. **385**, 18 (2009).
[43] B. B. Karki, R. M. Wentzcovitch, S. de Gironcoli, and S. Baroni, Phys. Rev. B **61**, 8793 (2000).
[44] B. B. Karki, R. M. Wentzcovitch, S. de Gironcoli, and S. Baroni, Phys. Rev. B **62**, 14750 (2000).
[45] P. Piekarz, P. T. Jochym, K. Parlinski, and J. Łazewski, J. Chem. Phys. **117**, 3340 (2002).
[46] Y. Xu, L. Zhang, T. Cui, Y. Li, Y. Xie, W. Yu, Y. Ma, and G. Zou, Phys. Rev. B **76**, 214103 (2007).
[47] H.-Y. Wang, H. Xu, T.-T. Huang, and C.-S. Deng, Eur. Phys. J. B **62**, 39 (2008).
[48] I. Hamdi, M. Aouissi, A. Qteish, and N. Meskini, Phys. Rev. B **73**, 174114 (2006).
[49] P. Brüsch, *Phonons: Theory and Experiments I* (Springer-Verlag, Berlin, New York, 1982).
[50] Y. Wang, Z.-K. Liu, and L.-Q. Chen, Acta Mater. **52**, 2665 (2004).
[51] R. E. Watson and M. Weinert, Phys. Rev. B **30**, 1641 (1984).
[52] X. Gonze *et al.*, Comput. Phys. Commun. **180**, 2582 (2009).
[53] S. Goedecker, SIAM J. Sci. Comput. (USA) **18**, 1605 (1997).
[54] M. C. Payne, M. P. Teter, D. C. Allan, T. A. Arias, and J. D. Joannopoulos, Rev. Mod. Phys. **64**, 1045 (1992).
[55] X. Gonze, Phys. Rev. B **54**, 4383 (1996).
[56] X. Gonze, Phys. Rev. B **55**, 10337 (1997).
[57] X. Gonze and C. Lee, Phys. Rev. B **55**, 10355 (1997).
[58] D. R. Hamann, X. Wu, K. M. Rabe, and D. Vanderbilt, Phys. Rev. B **71**, 035117 (2005).
[59] N. Troullier and J. L. Martins, Phys. Rev. B **43**, 1993 (1991).
[60] J. P. Perdew and Y. Wang, Phys. Rev. B **45**, 13244 (1992).
[61] http://opium.sourceforge.net/
[62] H. J. Monkhorst and J. D. Pack, Phys. Rev. B **13**, 5188 (1976).
[63] P. Vinet, J. H. Rose, J. Ferrante, and J. R. Smith, J. Phys.: Condens. Matter **1**, 1941 (1989).
[64] C. H. Booth, J. L. Sarrao, M. F. Hundley, A. L. Cornelius, G. H. Kwei, A. Bianchi, Z. Fisk, and J. M. Lawrence, Phys. Rev. B **63**, 224302 (2001).
[65] N. Sirota, V. Novikov, V. Vinokurov, and Y. Paderno, Phys. Solid State **40**, 1856 (1998).
[66] N. Sirota, V. Novikov, and A. Novikov, Phys. Solid State **42**, 2093 (2000).
[67] S. Sato, J. Magn. Magn. Mater. **52**, 310 (1985).
[68] B. K. Godwal, E. A. Petruska, S. Speziale, J. Yan, S. M. Clark, M. B. Kruger, and R. Jeanloz, Phys. Rev. B **80**, 172104 (2009).
[69] M. Ishii, T. Tanaka, E. Bannai, and S. Kawai, J. Phys. Soc. Jpn. **41**, 1075 (1976).
[70] H. Scholz, W. Bauhofer, and K. Ploog, Solid State Commun. **18**, 1539 (1976).
[71] Z. Yahia, S. Turrell, J.-P. Mercurio, and G. Turrell, J. Raman Spectrosc. **24**, 207 (1993).
[72] K. Kojima, K. Ohbayashi, T. Hihara, S. Kunii, T. Komatsubara, and T. Kasuya, Phys. Lett. A **72**, 51 (1979).
[73] M. Udagawa *et al.*, J. Phys. Soc. Jpn. **71**, 314 (2002), Supplement.
[74] S. Kunii, J. Phys. Soc. Jpn. **57**, 361 (1988).
[75] G. Schell, H. Winter, H. Rietschel, and F. Gompf, Phys. Rev. B **25**, 1589 (1982).
[76] E. Zirngiebl, H. Woike, S. Blumenroder, G. Guntherodt, A. Heidel, and R. R. Arons, J. Magn. Magn. Mater. **54-57**, 443

(1986).
[77] E. F. Westrum, Jr., J. T. S. Andrews, B. H. Justice, and D. A. Johnson, J. Chem. Thermodyn. **34**, 239 (2002).
[78] M. Schlesinger, P. Liao, and K. Spear, J. Phase Equilib. **20**, 73 (1999).
[79] V. B. Muratov, A. S. Bolgar, P. I. Loboda, and V. V. Morozov, Powder Metall. Met. Ceram. **27**, 984 1988).
[80] E. F. Westrum, Jr., B. H. Justice, H. L. Clever, and D. A. Johnson, J. Therm Anal. Calorim. **70**, 361 (2002).
[81] T. Fujita, M. Suzuki, T. Komatsubara, S. Kunii, T. Kasuya, and T. Ohtsuka, Solid State Commun. **35**, 569 (1980).
[82] F. Körmann, A. Dick, B. Grabowski, B. Hallstedt, T. Hickel, and J. Neugebauer, Phys. Rev. B **78**, 033102 (2008).
[83] V. V. Novikov, Phys. Solid State **43**, 300 (2001).